

Crystalline structure of $0.65\text{BiFeO}_3-0.35\text{Ba}_{1-x}\text{Sr}_x\text{TiO}_3$ solid solutions in the vicinity of the morphotropic phase boundary

Maxim V. Silibin¹, Polina A. Sklyar², Vadim D. Zhivulko³, Sergey I. Latushko^{1,3},
Dmitry V. Zheludkevich^{1,3}, Dmitry V. Karpinsky^{1,3}

¹ National Research University "Moscow Institute of Electronic Technology", 1 Shokin Sq., Zelenograd, Moscow 124498, Russian Federation

² National University of Science and Technology "MISIS", 4-1 Leninsky Ave., Moscow 119049, Russian Federation

³ Scientific-Practical Materials Research Centre of the National Academy of Sciences of Belarus, 19 P. Brovki Str., Minsk 220072, Republic of Belarus

Corresponding author: Dmitry V. Karpinsky (dmitry.karpinsky@gmail.com)

Received 31 July 2023 ♦ Accepted 9 October 2023 ♦ Published 12 December 2023

Citation: Silibin MV, Sklyar PA, Zhivulko VD, Latushko SI, Zheludkevich DV, Karpinsky DV (2023) Crystalline structure of $0.65\text{BiFeO}_3-0.35\text{Ba}_{1-x}\text{Sr}_x\text{TiO}_3$ solid solutions in the vicinity of the morphotropic phase boundary. *Modern Electronic Materials* 9(4): 193–200. <https://doi.org/10.3897/j.moem.9.4.116620>

Abstract

Complex transition metal oxides are distinguished for a close interrelation between their type of crystal structure and electrical and magnetic properties, thus determining their practical importance. Bismuth ferrite based solid solutions contain simultaneously both dipole electric and magnetic ordering thus expanding their potential applications as external impact sensors. The sensitivity of these compositions to external fields is largely dependent on their structural state. $0.65\text{BiFeO}_3-0.35\text{Ba}_{1-x}\text{Sr}_x\text{TiO}_3$ solid solutions ($0 \leq x \leq 1$) the compositions of which are close to the rhombohedral/cubic morphotropic phase boundary have metastable structures and are therefore promising functional materials. The crystal structure and morphology of $0.65\text{BiFeO}_3-0.35\text{Ba}_{1-x}\text{Sr}_x\text{TiO}_3$ solid solutions has been studied using X-ray diffraction, scanning electron microscopy, Raman spectroscopy and energy dispersive X-ray spectroscopy. The chemical substitution of barium ions for strontium ones has been found to reduce the magnitude of rhombohedral distortions and decrease the unit cell parameters for all the substituted compounds. Solid solutions with $x \geq 0.25$ have single-phase structure and cubic unit cells, their grain size decreasing with an increase in the concentration of the substituting ions. The results of structural studies obtained using Raman spectroscopy suggest the presence of rhombohedral distortions in the structures of all the compositions studied. The results of structural studies have allowed identifying the sequence of changes in the phase state and lattice parameter of the compounds in the vicinity of the rhombohedral/cubic morphotropic phase boundary. The concentration ranges in which the compounds have single-phase and two-phase structures have been found. The concentration stability range of the polar rhombohedral phase has been corrected on the basis of the structural data obtained using local and microscopic methods.

Keywords

bismuth ferrite, multiferroics, X-ray diffraction, electron microscopy, structural phase transitions, morphotropic phase boundary

1. Introduction

In the last decade multiferroics raise growing interest of researchers in the field of new functional materials. Multiferroics are well-known due to the possibility of controlling their properties originating from a close interrelation between their electric and magnetic subsystems, allowing to develop new materials offering new opportunities of practical applications [1–4]. For example, multiferroics are used for the construction of memory cells, in ferromagnetic resonance based devices and actuators, and as the working elements of external impact sensors (pressure, electric and magnetic fields). The choice of materials having several types of ferrite ordering is limited since strong dipole and magnetic ordering cannot coexist in oxides [2, 5, 6]. Therefore the search and development of new functional materials on the basis of complex transition metal oxides is an important task of modern materials science.

Bismuth ferrite (BiFeO_3) based solid solutions are the most renowned and promising single-phase multiferroics because their transition to magnetically ordered and ferroelectric states occurs at high temperatures: the Neel temperature $T_N \sim 650$ K and the Curie temperature $T_C \sim 1100$ K [2, 7]. It is well-known that the chemical substitution of bismuth and iron ions allows modifying the crystalline structure of BiFeO_3 based compounds and therefore controlling their physical properties, magnetization, specific resistivity, electromechanical and magnetoelectric properties [8–12].

The magnitude of the magnetoelectric effect in bismuth ferrite based multiferroics is but moderate ($\sim 10\text{--}100$ mV/cm/Oe) as compared with that for composites [13–16]. However, there are indications that the formation of bismuth ferrite based solid solutions the compounds of which are close to the morphotropic phase boundaries improves their performance [9, 17, 18]. For example, substitution of bismuth ions for barium and strontium ones and iron ions for titanium ones in bismuth ferrite is an efficient way to form electro- and magnetostrictive components in single-phase multiferroics [19–21]. The properties of these solid solutions are largely determined by the percolation phenomenon which involves anomalous changes in the electric and magnetic properties of the materials in the vicinity of the phase boundary where interpenetration of the phases occurs. Percolation boundaries largely depend on the grain size of the solid solutions, and there are but a few works dealing with the effect of the structural state on the improvement of the physicochemical properties of bismuth ferrite based solid solutions.

The available literary works dealing with the structural phase transitions in the $\text{BiFeO}_3\text{--Ba(Sr)TiO}_3$ systems often provide contradictory data on the concentration stability ranges of the coexisting structural phases. Furthermore, there are no convincing experimental data on the ratio between the magnetically active and ferroelectric subsystems in those solid solutions and on the formation

conditions of metastable structural states in compounds close to the morphotropic phase boundaries. Presented below are data on the rhombohedral-to-cubic structural phase transition in the $0.65\text{BiFeO}_3\text{--}0.3\text{Ba}_{1-x}\text{Sr}_x\text{TiO}_3$ system of solid solutions ($0 \leq x \leq 1$). The data broaden the understanding of the structure of the bismuth ferrite based solid solutions and will favor the development and synthesis of new functional materials exhibiting magnetoelectric interaction.

2. Experimental

Ceramic specimens of the $0.65\text{BiFeO}_3\text{--}0.3\text{Ba}_{1-x}\text{Sr}_x\text{TiO}_3$ system ($x = 0, 0.15, 0.25, 0.5, 0.75$ and 1) were synthesized using the method of solid phase reactions. The raw materials were high-purity oxides and carbonates BaCO_3 , SrCO_3 , Bi_2O_3 , Fe_2O_3 and La_2O_3 . The mixture of oxides taken in the stoichiometric ratio was crushed for 60 min in an ethyl alcohol media in a RETSCH 200 PM planetary mill. The resultant powders were uniaxially pressed at 0.1 GPa to 10 mm diam. 1–2 mm thick tablets. After intermediate crushing and compressing the specimens were synthesized for 10 h at 1000–1050 °C with a gradual increase in the synthesis temperature and an increase in the concentration of the dopant ions. The specimens were then quenched from the synthesis temperature to room temperature at a 100–200 K/s cooling rate.

X-ray phase and structural studies were conducted using an Adani PowDiX 600 X-ray diffractometer (CuK_α radiation, wavelength $\lambda = 0.15406$ nm) at room temperature. The K_β component was cut off with a graphite monochromator. The spectra were recorded in the Bragg–Brentano setup. The X-ray patterns were taken in the 20 to 60 deg. 2θ range with a 0.02 deg. scanning step. The X-ray data were analyzed using the Rietveld method (full-profile analysis). The spectra were refined with the FullProf software.

The grain morphology was studied under a Zeiss Evo 10 scanning electron microscope and the elemental composition of the specimens was analyzed using energy dispersive X-ray spectroscopy on an Oxford Instruments EDS attachment. The Raman spectra were recorded on a Confotec MR350 spectrometer (SOL Instruments, Belarus) with 532 nm excitation radiation.

3. Results and discussion

3.1. Crystalline structure of $0.65\text{BiFeO}_3\text{--}0.3\text{Ba}_{1-x}\text{Sr}_x\text{TiO}_3$ solid solutions

Analysis of the X-ray diffraction patterns (Fig. 1) suggests that all the experimental solid solutions are free from impurity phases accurate to the methodical error (~ 1 mol.%). Rietveld refining of the diffraction data showed the change in the crystalline structure depend-

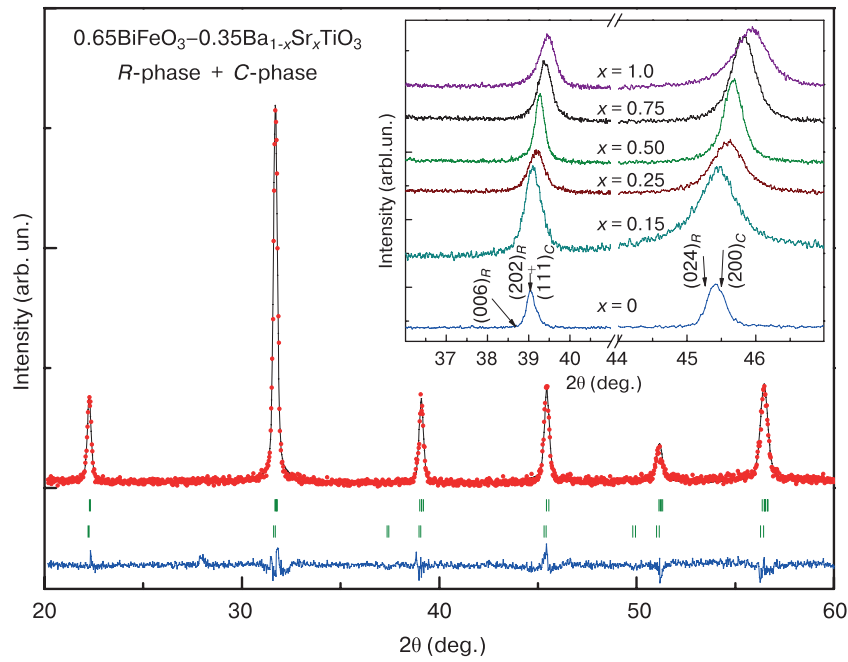


Figure 1. Room-temperature X-ray diffraction pattern of $0.65\text{BiFeO}_3\text{-}0.35\text{BaTiO}_3$ solid solution composition ($x = 0$) refined in the two-phase model (space groups $R3c$ and $Pm\bar{3}m$). Inset: X-ray diffraction patterns showing reflections typical of (C) cubic and (R) rhombohedral phases with compositions $0.65\text{BiFeO}_3\text{-}0.35\text{Ba}_{1-x}\text{Sr}_x\text{TiO}_3$ where $x = 0, 0.25, 0.5, 0.75$ and 1.0

ing on the concentration of the dopant ions. A sequence of changes in the structural parameters and the volume fractions of the structural phases was identified. The X-ray data for the $\text{Bi}_{0.65}\text{Ba}_{0.35}\text{Fe}_{0.65}\text{Ti}_{0.35}\text{O}_3$ solid solution ($x = 0$) suggest the presence of two phases: a polar rhombohedral one (space group $R3c$) and a cubic one ($Pm\bar{3}m$). The cubic phase dominates, the volume fraction of the rhombohedral one being ~ 10 vol.%. The $\text{Bi}_{0.65}\text{Ba}_{0.2975}\text{Sr}_{0.0525}\text{Fe}_{0.65}\text{Ti}_{0.35}\text{O}_3$ solid solution ($x = 0.15$) also contains two phases, the volume fraction of the rhombohedral phase being below ~ 5 vol.%. This mixed

structural state containing two phases with close unit cell parameters causes broadening of the diffraction peaks (Fig. 1) and hence complicates accurate calculation of the structural parameters for these phases. Further increase in the concentration of Sr ions causes a structural transition to the single cubic phase state as shown by the evolution of the typical reflections associated with distortion of oxygen octahedra in the ab plane of the rhombohedral lattice (Fig. 1). Figure 1 shows the X-ray diffraction patterns of the $0.65\text{BiFeO}_3\text{-}0.35\text{Ba}_{1-x}\text{Sr}_x\text{TiO}_3$ solid solutions with $0 \leq x \leq 1$. Analysis of the X-ray diffraction

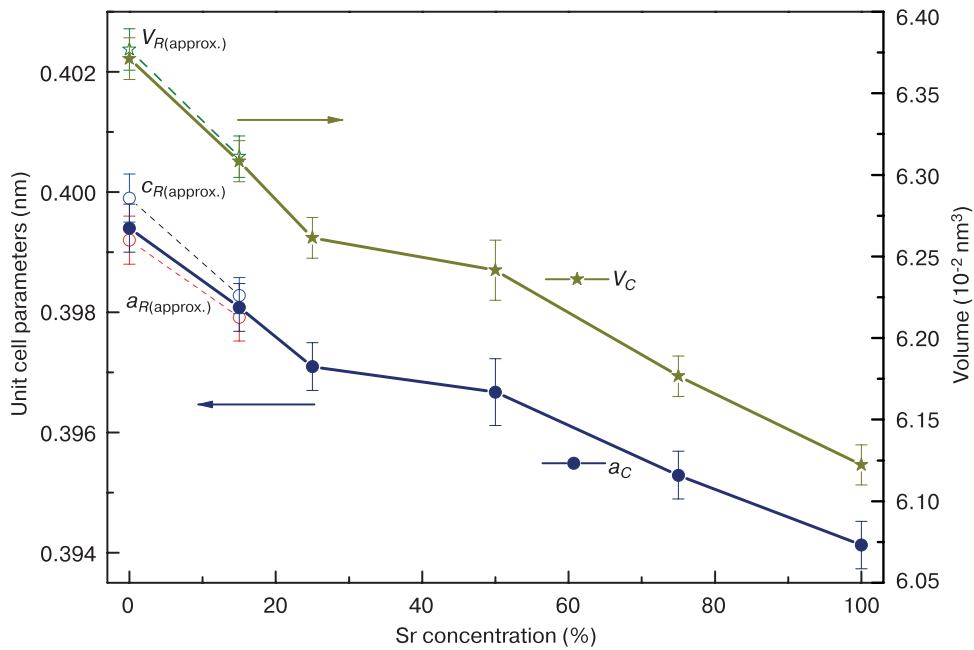


Figure 2. Unit cell parameters for $0.65\text{BiFeO}_3\text{-}0.35\text{Ba}_{1-x}\text{Sr}_x\text{TiO}_3$ compounds

patterns showed that all the experimental solid solutions undergo slight structural changes. The compound with $x = 1$ still exhibits some asymmetry of the reflections, probably indicating an inhomogeneous structural state of the compounds on local scale. The solid solution of this compound is single phase and has a cubic unit cell. The concentration phase transition to the cubic structure is accompanied by a decrease in the lattice parameters and hence the unit cell volume from $V \sim 63.71 \cdot 10^{-3} \text{ nm}^3$ and $63.73 \cdot 10^{-3} \text{ nm}^3$ (the values are shown for the cubic and rhombohedral phases, respectively) for the $0.65\text{BiFeO}_3\text{--}0.35\text{BaTiO}_3$ composition to $61.22 \cdot 10^{-3} \text{ nm}^3$ for the $0.65\text{BiFeO}_3\text{--}0.35\text{SrTiO}_3$ composition. The decrease in the lattice parameters is caused by the substitution of the Ba ions with a large ionic radius ($r(\text{Ba}_{\text{VI}}^{2+}) = 0.135 \text{ nm}$) for the Sr ions with a smaller ionic radius ($r(\text{Sr}_{\text{VI}}^{2+}) = 0.118 \text{ nm}$). Noteworthy, the iron Fe^{3+} and titanium Ti^{4+} ions have close ionic radii in an octahedral neighborhood ($r(\text{Fe}_{\text{VI}}^{3+}) = 0.0645 \text{ nm}$ and $r(\text{Ti}_{\text{VI}}^{4+}) = 0.0605 \text{ nm}$), and the ionic radius of the Bi^{3+} ions is 0.117 nm for the coordination number $\text{CN} = 12$ which is typical of the rhombohedral unit cell.

The change of the lattice parameters (Fig. 2) suggests a monotonic reduction of the unit cell parameter, whereas the normalized rhombohedral phase unit cell volume of the initial $0.65\text{BiFeO}_3\text{--}0.35\text{BaTiO}_3$ compound is greater than that of the dominating cubic phase which is in agreement with the general trend of decreasing lattice parameters upon chemical substitution for strontium ions. The

anomalous change of the unit cell parameter for the compound with $x = 0.5$ is possibly caused by the formation of oxygen vacancies during specimen cooling after synthesis which is in agreement with the energy dispersion data. Barium ion substitution for strontium ions causes a general decrease in the unit cell volume by $\sim 3.7\%$ (the difference in the ionic radii of barium and strontium is $\sim 14\%$). Taking into account the chosen substitution model ($0.65\text{BiFeO}_3\text{--}0.35\text{Ba}_{1-x}\text{Sr}_x\text{TiO}_3$), this suggests that the dimensional effect influences the crystalline lattice parameters in an almost linear manner.

3.2. Grain morphology and chemical composition of $0.65\text{BiFeO}_3\text{--}0.35\text{Ba}_{1-x}\text{Sr}_x\text{TiO}_3$ solid solutions

The grain structure of the solid solutions was studied using scanning electron microscopy (SEM). Figure 3 shows SEM images for the $0.65\text{BiFeO}_3\text{--}0.35\text{Ba}_{1-x}\text{Sr}_x\text{TiO}_3$ compounds. The microstructure of the solid solutions slightly changes with an increase in the strontium ion concentration. The test compounds contain particle agglomerations sized from units to decades of microns consisting of round-shaped particles with linear sizes of ~ 0.2 to $\sim 2 \text{ }\mu\text{m}$. An increase in the concentration of Sr ions causes a monotonic decrease in the average grain size from $\sim 0.9 \text{ }\mu\text{m}$ for the compound with $x = 0.25$ to $\sim 0.63 \text{ }\mu\text{m}$ for the compound with $x = 1$. The compounds with $x < 0.5$ have almost constant average grain sizes, whereas for compounds with higher strontium ion concentrations the

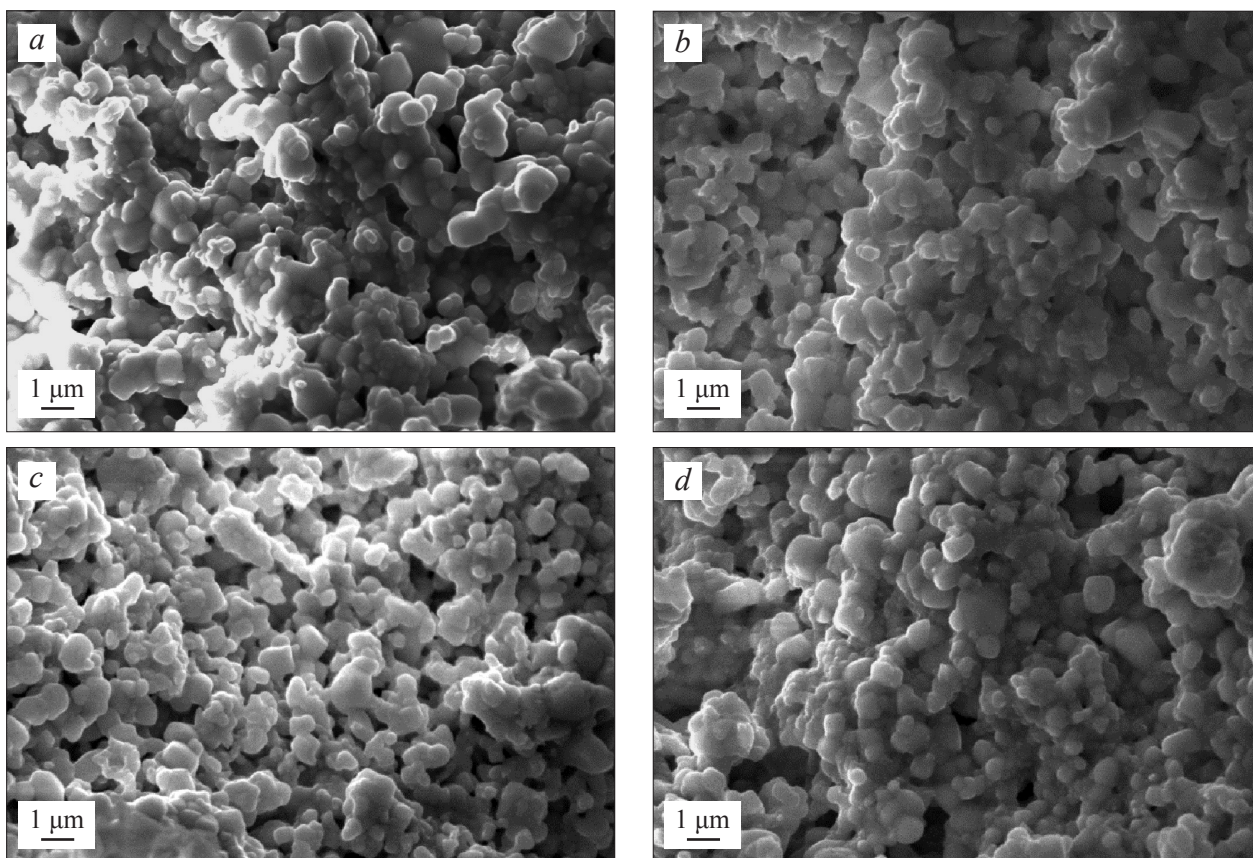


Figure 3. SEM images of $0.65\text{BiFeO}_3\text{--}0.35\text{Ba}_{1-x}\text{Sr}_x\text{TiO}_3$ solid solutions: (a) $x = 0.25$; (b) 0.5 ; (c) 0.75 ; (d) 1.0

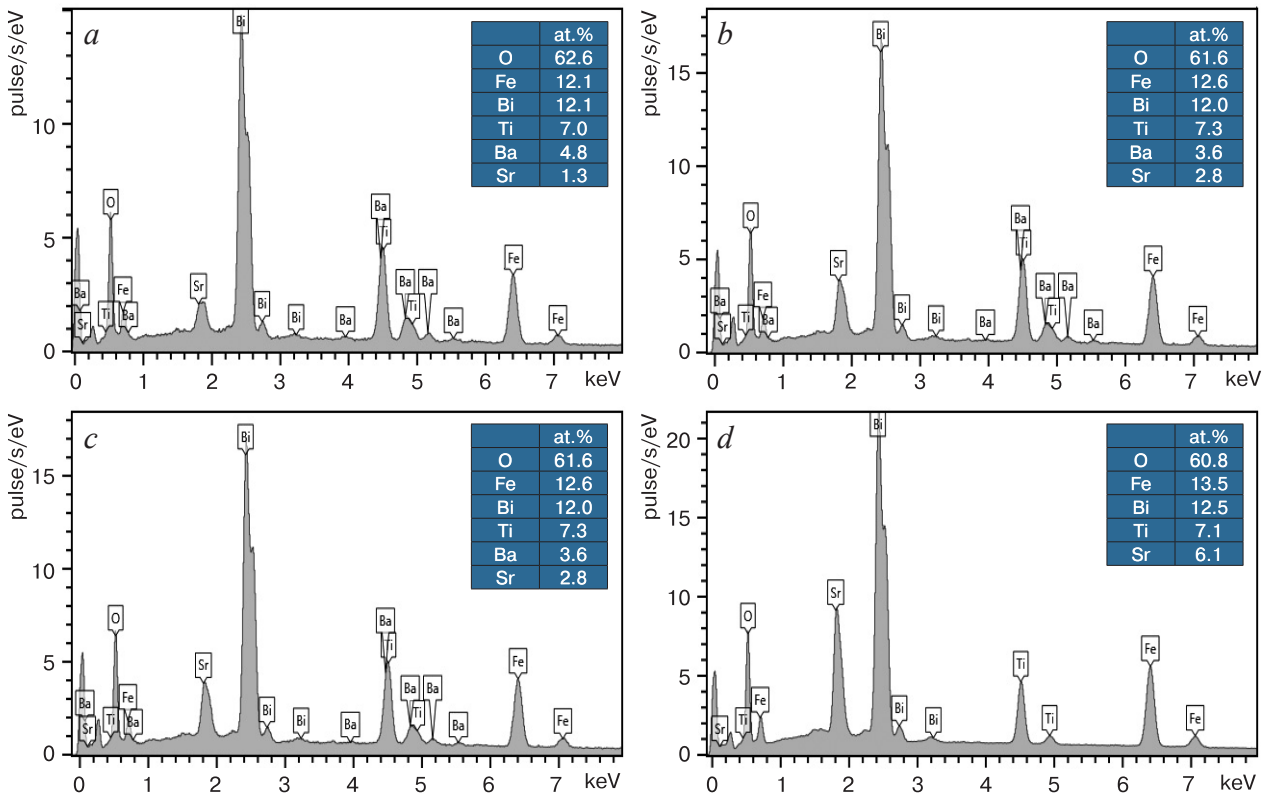


Figure 4. Energy dispersion X-ray spectra of $0.65\text{BiFeO}_3\text{--}0.35\text{Ba}_{1-x}\text{Sr}_x\text{TiO}_3$ solid solutions: (a) $x = 0.25$; (b) 0.5 ; (c) 0.75 ; (d) 1.0 . Insets show elemental compositions of specimens

average grain sizes decrease significantly. The shape of the grains is fairly insensitive to the chemical composition and structural state of the specimens, and therefore grains with different unit cell distortion types cannot be distinguished. The nonmonotonic decrease in the average grain size with an increase in the strontium ion concentration agrees with the diffraction peak broadening observed in the diffraction patterns of the solid solutions for the compositions with $x > 0.5$ (Fig. 1).

Elemental analysis of the $0.65\text{BiFeO}_3\text{--}0.35\text{Ba}_{1-x}\text{Sr}_x\text{TiO}_3$ system of solid solutions with $x = 0\div 1$ using energy dispersion X-ray spectroscopy suggests the absence of impurity phases, with the chemical composition of the specimens changing in accordance with the substitution model used. The presence of small quantities of the C and Al elements is caused by the experimental setup chosen (the specimens were attached to aluminum holders with carbon-containing tape). The concentration ratio of the main chemical elements confirms the rated chemical formulas for the $0.65\text{BiFeO}_3\text{--}0.35\text{Ba}_{1-x}\text{Sr}_x\text{TiO}_3$ system (data on the quantities of elements in the solid solutions are shown in insets of Fig. 4). The elemental analysis data suggest a high chemical homogeneity of the solid solutions. The difference in the contents of chemical elements for the composition with $x = 0$ which is two-phase is within 2% according to the X-ray data in different points of the surface studied, and therefore grains with different structural states cannot be distinguished. The rated content of oxygen ions is slightly above the stoichiometric one, probably due to the nanometer-level

sizes of the particles and their oxidation in air. Thus, the chemical formulas shown below were calculated from the energy dispersion data for the abovementioned four compositions (x).

x	$0.65\text{BiFeO}_3\text{--}0.35\text{Ba}_{1-x}\text{Sr}_x\text{TiO}_3$
0.17	$\text{Bi}_{0.579}\text{Ba}_{0.230}\text{Sr}_{0.062}\text{Fe}_{0.579}\text{Ti}_{0.335}\text{O}_3$
0.39	$\text{Bi}_{0.584}\text{Ba}_{0.175}\text{Sr}_{0.136}\text{Fe}_{0.614}\text{Ti}_{0.355}\text{O}_3$
0.67	$\text{Bi}_{0.546}\text{Ba}_{0.071}\text{Sr}_{0.235}\text{Fe}_{0.518}\text{Ti}_{0.339}\text{O}_3$
0.86	$\text{Bi}_{0.617}\text{Sr}_{0.301}\text{Fe}_{0.671}\text{Ti}_{0.350}\text{O}_3$

These formulas suggest a over-stoichiometric concentration of oxygen anions due to a deficiency of cations in the A and B perovskite sublattices, in agreement with literary data on the chemical composition of the $\text{BiFeO}_3\text{--}\text{BaTiO}_3$ solid solutions [22, 23].

3.3. Raman spectroscopy study of $0.65\text{BiFeO}_3\text{--}0.35\text{Ba}_{1-x}\text{Sr}_x\text{TiO}_3$ solid solutions

The X-ray diffraction data on the crystalline structure for solid solutions of different compositions were added with Raman spectroscopy data. The Raman spectroscopy data delivered additional information on the structure of the compounds on a local level (nanometers) and thus allowed assessing the degree and type of structural distur-

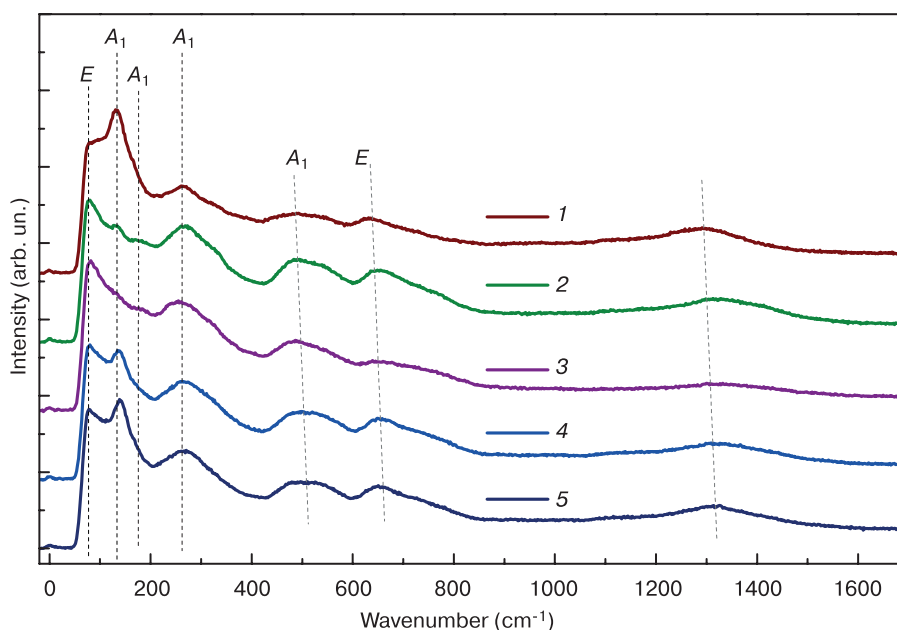


Figure 5. Raman spectra of $0.65\text{BiFeO}_3\text{-}0.35\text{Ba}_{1-x}\text{Sr}_x\text{TiO}_3$ solid solutions: (1) $x = 0$; (2) 0.25; (3) 0.5; (4) 0.75; (5) 1.0

tions in the oxygen octahedra, as well as the lengths and angles of the Bi(Ba,Sr)–O and Fe(Ti)–O chemical bonds.

It is well-known that the Raman spectra of solid solutions having a cubic perovskite structure do not contain first-order Raman modes. The data obtained in this work suggest the presence of active Raman modes and diffuse bands in the spectra, possibly due to second and higher orders Raman scattering (Fig. 5). The presence of narrow Raman modes in the spectra indicates the presence of local structural distortions in the solid solutions which can be caused by the formation of nanosized clusters with a lower than cubic symmetry.

Note that the initial BiFeO_3 composition with rhombohedral unit cell distortions exhibits typical active E(1TO), E(2TO), A1(1TO) and A1(2TO) Raman modes at 77, 136, 142 and 170 cm^{-1} , respectively, caused by bismuth ion oscillations in the oxygen cubic octahedra [24, 25]. The presence of the E(1TO) and A1(1TO) Raman modes that are typical of rhombohedral BiFeO_3 based solid solutions suggests that rhombohedral unit cell distortions persisted in all the test compositions. The Raman spectra of all the solid solutions had clear active Raman modes at 78 and 140 cm^{-1} , the intensity of the former mode increasing and the intensity of the latter one decreasing with an increase in the concentration of strontium ions. This redistribution of Raman mode intensities is caused by a decrease in the rhombohedral unit cell distortions and in the volume of the unit cell for both structural phases. The decrease in the intensity of the E(1) mode at 78 cm^{-1} is caused by a decrease in the oscillation amplitude of the Bi(Ba,Sr)–O ions in the a - b plane of the rhombohedral cell, and the change in the intensity of the A(1) mode at 140 cm^{-1} originates from the Bi(Ba,Sr)–O oscillations along the c axis of the rhombohedral cell [26], the frequency of all the active modes increasing due to a decrease in the lattice parameters.

The presence of the diffuse bands at 275, 510, 650 and 1320 cm^{-1} can be caused either by two-phonon scattering processes or by oxygen anion tension-compression oscillation modes.

An increase in the concentration of strontium ions does not cause any significant changes to the main bands in the Raman spectra, this suggesting that the main structural state of the test solid solutions persists. With an increase in the concentration of strontium ions, the A(1TO) band shifts towards higher frequencies, indicating a change in the type of the Bi(Ba,Sr)–O bonds due to barium ion substitution for lighter strontium ions. Noteworthy, the uneven broadening of diffraction peaks observed in the X-ray diffraction patterns agrees with the structural model assuming that a matrix having a paraelectric cubic structure can contain nanosized clusters with rhombohedral unit cell distortions.

4. Conclusion

$0.65\text{BiFeO}_3\text{-}0.35\text{Ba}_{1-x}\text{Sr}_x\text{TiO}_3$ system solid solutions with $x = 0, 0.15, 0.25, 0.5, 0.75$ and 1 corresponding to the region in the vicinity of the rhombohedral/cubic morphotropic phase boundary were synthesized using the method of solid phase reactions. The crystal structure and morphology of the solid solutions were studied using microscopic and local methods. The substitution of barium ions for strontium ones reduces the degree of rhombohedral distortions and leads to a decrease in the lattice parameters. It was shown that the solid solutions with $x = 0$ and 0.15 are in a two-phase structural state in which a polar rhombohedral structure and a cubic structure coexist, and the solid solutions with $x = 0.25$ are single-phase with a perovskite cubic structure. An increase in the concentration of strontium ions to $x = 0.5$ reduces the aver-

age grain size but slightly, while for the compounds with higher strontium ion concentrations the average grain size decreases much faster due to a lower chemical activity of strontium ions compared with those of bismuth and barium ions and an increase in the number of oxygen vacancies in the solid solutions with $x > 0.5$ which reduces grain growth during synthesis.

For all the test compounds Raman spectroscopy showed the presence of local distortions typical of compounds with a rhombohedral structure. The X-ray diffraction and Raman scattering structural data indicate the formation of inhomogeneous structural states in the solid solutions, i.e., the main matrix having a paraelectric cubic

structure contains polar-active nanosized clusters with rhombohedral unit cell distortions.

Acknowledgements

The work was carried out with support of the Russian Science Foundation (grant No. 23-19-00347); the electron microscopic experiments were conducted with support from the Belarus Republican Foundation for Fundamental Research.

References

- Banoth P., Narsaiah B.P., De Los Santos Valladares L., Kargin J., Kollu P. Single-phase BiFeO₃ and BiFeO₃-Fe₂O₃ nanocomposite photocatalysts for photodegradation of organic dye pollutants. *Nanoscale Advances*. 2023; 5(9): 2646–2656. <https://doi.org/10.1039/d2na00881e>
- Catalan G., Scott J.F. Physics and applications of bismuth ferrite. *Advanced Materials*. 2009; 21(24): 2463–2485. <https://doi.org/10.1002/adma.200802849>
- Banoth P., Sohan A., Kandula C., Kollu P. Structural, dielectric, magnetic, and ferroelectric properties of bismuth ferrite (BiFeO₃) synthesized by a solvothermal process using hexamethylenetetramine (HMTA) as precipitating agent. *Ceramics International*. 2022; 48(22): 32817–32826. <http://dx.doi.org/10.2139/ssrn.4084619>
- Pyatakov A.P., Zvezdin A.K. Magnetoelectric and multiferroic media. *Physics-Uspeski*. 2012; 55(6): 557. <https://doi.org/10.3367/UFNe.0182.201206b.0593>
- Chu Y.H., Martin L.W., Holcomb M.B., Ramesh R. Controlling magnetism with multiferroics. *Materials Today*. 2007; 10(10): 16–23. [http://dx.doi.org/10.1016/S1369-7021\(07\)70241-9](http://dx.doi.org/10.1016/S1369-7021(07)70241-9)
- Sando D., Barthélémy A., Bibes M. BiFeO₃ epitaxial thin films and devices: past, present and future. *Journal of Physics: Condensed Matter*. 2014; 26(47): 473201. <https://doi.org/10.1088/0953-8984/26/47/473201>
- Fischer P., Polomska M., Sosnowska I., Szymanski M. Temperature dependence of the crystal and magnetic structures of BiFeO₃. *Journal of Physics C: Solid State Physics*. 1980; 13(10): 1931. <https://doi.org/10.1088/0022-3719/13/10/012>
- Phong P.T., Salazar-Kuri U., Van H.T., Khien N.V., Dang N.V., Tho P.T. Influence of isothermal structural transition on the magnetic properties of Cr doped Bi_{0.86}Nd_{0.14}FeO₃ multiferroics. *Journal of Alloys and Compounds*. 2020; 823: 153887. <https://doi.org/10.1016/j.jallcom.2020.153887>
- Tho P.T., Clements E.M., Kim D.H., Tran N., Osofsky M.S., Phan M.-H., Phan T.L., Lee B.W. Crystal structure and magnetic properties of Ti-doped Bi_{0.84}La_{0.16}FeO₃ at morphotropic phase boundary. *Journal of Alloys and Compounds*. 2018; 741: 59–64. <https://doi.org/10.1016/j.jallcom.2018.01.140>
- Karpinsky D.V., Troyanchuk I.O., Tovar M., Sikolenko V., Efimov V., Efimova E., Shur V.Ya., Kholkin A.L. Temperature and composition-induced structural transitions in Bi_{1-x}La(Pr)_xFeO₃ ceramics. *Journal of the American Ceramic Society*. 2014; 97(8): 2631–2638. <https://doi.org/10.1111/jace.12978>
- Karpinsky D.V., Troyanchuk I.O., Sikolenko V., Efimov V., Efimova E., Willinger M., Salak A.N., Kholkin A.L. Phase coexistence in Bi_{1-x}(Pr)_xFeO₃ ceramics. *Journal of Materials Science*. 2014; 49(20): 6937–6943. <https://doi.org/10.1007/s10853-014-8398-6>
- Khomchenko V.A., Troyanchuk I.O., Karpinsky D.V., Das S., Amaral V.S., Tovar M., Sikolenko V., Paixão J.A. Structural transitions and unusual magnetic behavior in Mn-doped Bi_{1-x}La_xFeO₃ perovskites. *Journal of Applied Physics*. 2012; 112(8): 084102. <https://doi.org/10.1063/1.4759435>
- Kitagawa Y., Hiraoka Y., Honda T., Ishikura T., Nakamura H., Kimura T. Low-field magnetoelectric effect at room temperature. *Nature Materials*. 2010; 9(10): 797–802. <https://doi.org/10.1038/nmat2826>
- Singh A., Pandey V., Kotnala R.K., Pandey D. Direct evidence for multiferroic magnetoelectric coupling in 0.9BiFeO₃-0.1BaTiO₃. *Physical Review Letters*. 2008; 101(24): 247602. <https://doi.org/10.1103/PhysRevLett.101.247602>
- López I., Castaldini A., Cavallini A., Nogales E., Méndez B., Piqueras J. β-Ga₂O₃ nanowires for an ultraviolet light selective frequency photodetector. *Journal of Physics D: Applied Physics*. 2014; 47(41): 415101. <https://doi.org/10.1088/0022-3727/47/41/415101>
- Li Y., Sun N., Liu J., Hao X., Du J., Yang H., Li X., Cao M. Multifunctional BiFeO₃ composites: absorption attenuation dominated effective electromagnetic interference shielding and electromagnetic absorption induced by multiple dielectric and magnetic relaxations. *Composites Science and Technology*. 2018; 159: 240–250. <https://doi.org/10.1016/j.compscitech.2018.02.014>
- Ca N.X., Lee M.Y., Nguyen H., Ba D.N., Tho P.T., Dang N.V., Tran N., Lee B.W., Ha L.T., Hue L.T., Chu X. Peculiar magnetism of Bi_{1-x}Dy_xFeO₃ ceramics at the morphotropic phase boundary. *Journal of Alloys and Compounds*. 2021; 869: 159331. <https://doi.org/10.1016/j.jallcom.2021.159331>

18. Karpinsky D.V., Troyanchuk I.O., Trukhanov A.V., Willinger M., Khomchenko V.A., Kholkin A.L., Sikolenko V., Maniecki T., Maniekiewicz W., Dubkov S.V., Silibin M.V. Structure and piezoelectric properties of Sm-doped BiFeO_3 ceramics near the morphotropic phase boundary. *Materials Research Bulletin*. 2019; 112: 420–425. <https://doi.org/10.1016/j.materresbull.2018.08.002>
19. Pakalniškis A., Lukowiak A., Niaura G., Gluchowski P., Karpinsky D.V., Alikin D.O., Abramov A.S., Zhaludkevich A., Silibin M.V., Kholkin A.L., Skaudžius R., Strek W., Kareiv A. Nanoscale ferroelectricity in pseudo-cubic sol-gel derived barium titanate-bismuth ferrite ($\text{BaTiO}_3\text{-BiFeO}_3$) solid solutions. *Journal of Alloys and Compounds*. 2020; 830: 154632. <https://doi.org/10.1016/j.jallcom.2020.154632>
20. Reetu R., Agarwal A., Sanghi S., Ashima A. Rietveld analysis, dielectric and magnetic properties of Sr and Ti codoped BiFeO_3 multiferroic. *Journal of Applied Physics*. 2011; 110(7): 073909. <https://doi.org/10.1063/1.3646557>
21. Liu H., Yang X. Structural, dielectric, and magnetic properties of $\text{BiFeO}_3\text{-SrTiO}_3$ solid solution ceramics. *Ferroelectrics*. 2016; 500(1): 310–317. <https://doi.org/10.1080/00150193.2016.1230445>
22. Tang L., Zhou X., Habib M., Zou J., Yuan X., Zhang Y., Zhang D. Phase structure and electrical properties of $\text{BiFeO}_3\text{-BaTiO}_3$ ceramics near the morphotropic phase boundary. *Ceramics International*. 2023; 49(24): 31965–31974. <https://doi.org/10.1016/j.ceramint.2023.07.160>
23. Kim S., Khanal G.P., Nam H.-W., Fujii I., Ueno S., Moriyoshi C., Kuroiwa Y., Wada S. Structural and electrical characteristics of potential candidate lead-free $\text{BiFeO}_3\text{-BaTiO}_3$. *Journal of Applied Physics*. 2017; 122(16): 164105. <https://doi.org/10.1063/1.4999375>
24. Hlinka J., Pokorný J., Karimi S., Reaney I.M. Angular dispersion of oblique phonon modes in from micro-Raman scattering. *Physical Review B*. 2011; 83(2): 020101. <https://doi.org/10.1103/PhysRevB.83.020101>
25. Wang Y., Nan C.-W. Site modification in BiFeO_3 thin films studied by Raman spectroscopy and piezoelectric force microscopy. *Journal of Applied Physics*. 2008; 103(11): 114104. <https://doi.org/10.1063/1.2938080>
26. Hermet P., Goffinet M., Kreisel J., Ghosez P. Raman and infrared spectra of multiferroic bismuth ferrite from first principles. *Physical Review B*. 2007; 75(22): 220102 (R). <https://doi.org/10.1103/PhysRevB.75.220102>